Research Paper

GEOSPHERE

GEOSPHERE, v. 15, no. 2

https://doi.org/10.1130/GES01520.1

5 figures; 1 table

CORRESPONDENCE: pangjz@ies.ac.cn

CITATION: Yu, J.X., Pang, J.Z., Wang, Y.Z., Zheng, D.W., Liu, C.C., Wang, W.T., Li, Y.J., Li, C.P., and Xiao, L., 2019, Mid-Miocene uplift of the northern Qilian Shan as a result of the northward growth of the northern Tibetan Plateau: Geosphere, v. 15, no. 2, p. 423–432, https://doi.org/10.1130/GES01520.1.

Science Editor: Raymond M. Russo

Received 1 March 2017
Revision received 9 October 2018
Accepted 5 December 2018

Published online 16 January 2019

GOLD OPEN ACCESS

THE GEOLOGICAL SOCIETY OF AMERICA®

This paper is published under the terms of the CC-BY-NC license.

© 2019 The Authors

# Mid-Miocene uplift of the northern Qilian Shan as a result of the northward growth of the northern Tibetan Plateau

**Jingxing Yu[1,2], Jianzhang Pang[1], Yizhou Wang[1], Dewen Zheng[1,3], Caicai Liu[1], Weitao Wang[4,1], Youjuan Li[1], Chaopeng Li[1], and Lin Xiao[1]**

[1]State Key Laboratory of Earthquake Dynamics, Institute of Geology, China Earthquake Administration, Beijing 100029, China
[2]Centre for the Observation and Modelling of Earthquakes, Volcanoes and Tectonics (COMET), Department of Earth Sciences, University of Oxford, Oxford OX1 3AN, UK
[3]Guangzhou Institute of Geochemistry, Chinese Academy of Sciences, Guangzhou 510640, China
[4]School of Earth Sciences and Engineering, Sun Yat-Sen University, Guangzhou 510275, China

## ABSTRACT

**The northern Tibetan Plateau, north of the Qaidam Basin and south of the Hexi Corridor (China), consists of a series of WNW- to NW-trending elongated mountain ranges. Deciphering the time-space deformation pattern of these ranges is central to understanding the mechanism of plateau formation and to the controversial issue of whether Tibet has undergone progressive northward growth or synchronous growth since the India-Eurasia collision. Here, we report new constraints on the timing of accelerated uplift of the Tuolai Shan, one of the elongated mountain ranges in the northern Tibetan Plateau. New apatite fission-track data from an elevation transect in the Tuolai Shan provide a definitive tie to rapid cooling that began at 17–15 Ma. We attribute this rapid cooling to accelerated exhumation resulting from thrusting in the hanging wall of the Haiyuan fault in response to progressive northward growth of the plateau. Combining these fission-track data and the published geologic, sedimentological, and thermochronologic data from the northern Qilian Shan and Hexi Corridor, we propose a progressively north-northeastward growth model for the northernmost part of Tibet, suggesting that deformation in the inner Qilian Shan occurred synchronously in the middle Miocene, and subsequently, increasingly further north.**

## INTRODUCTION

The collision between India and Eurasia resulted in widespread deformation throughout the continental interior of Eurasia, producing the crust-thickened Tibetan Plateau and its deformed surrounding regions (e.g., Molnar and Tapponnier, 1975; Tapponnier and Molnar, 1979). Two end-member models have been developed to explain the deformation of the Tibetan lithosphere, namely the rigid-block model (e.g., Tapponnier et al., 2001) and the continuum lithospheric deformation model (e.g., England and Houseman, 1986). When and how the plateau grew to its present elevation remain the essential unanswered questions to understanding the deformation mechanism(s) of the Tibetan lithosphere. Several prior works concluded that early, collision-age deformation occurred not only in southern Tibet near the India-Eurasia collision zone, but also in northern Tibet (e.g., Clark et al., 2010; Clark, 2012; Dayem et al., 2009), whereas others share the view that crustal thickening resulting from India's northward advance into Eurasia has propagated northward in time, first accumulating at the plate boundary and starting in the Miocene to Plio-Quaternary in northern Tibet (e.g., Meyer et al., 1998; Tapponnier et al., 2001; Royden et al., 2008; Molnar and Stock, 2009). Although a growing body of evidence for the deformation timing and styles in different parts of Tibet has been achieved, further work is needed to understand the mechanism of crustal thickening of the plateau.

Northern Tibet, located north of the eastern Kunlun Shan and Qaidam Basin and to the south of the Hexi Corridor and Gobi Alashan block (China), is dominated by crustal strike slip and overthrusting (Fig. 1). The most impressive geomorphic feature of the northern Tibetan Plateau is a series of WNW- or NW-trending ranges, e.g., the Zoulang Nan Shan, Tuolai Shan, Tuolai Nan Shan, Shule Nan Shan, Danghe Nan Shan, and Qaidam Shan, which are separated by subparallel elongated intermountain basins, e.g., the Changma, Qilian, Menyuan, and Hala Lake Basins (Meyer et al., 1998; Tapponnier et al., 2001). These elongated ranges and intermountain basins are typically bounded by growing folds and active thrusts (e.g., Tapponnier et al., 1990; Meyer et al., 1998; Yuan et al., 2013) that are linked to the accommodation of motion of the Altyn Tagh fault through transfer of left-lateral strike-slip motion to oblique thrusting (Burchfiel et al., 1989; Meyer et al., 1998). Several studies have been conducted to constrain the depositional histories and evolution of these intermountain basins, suggesting both earlier Cenozoic tectonic activity during the Eocene–Oligocene (e.g., Dupont-Nivet et al., 2004; Horton et al., 2004; Dai et al., 2006) and Miocene crustal shortening in the northern Tibetan Plateau (e.g., Fang et al., 2003, 2007; Lease et al., 2012; Wang et al., 2011, 2013, 2016a, 2016b). Thermochronologic exhumation records in the elongated mountain ranges show that uplift occurred both in the early Cenozoic, during the Eocene (e.g., Jolivet et al., 2001; Clark et al., 2010; Duvall et al., 2011), and also in the late Cenozoic (e.g., George et al., 2001; Zheng et al., 2006, 2010; Lease et al., 2011). Because these constraints on the timing of initial deformation are inconsistent, it remains controversial as to whether the northern Tibetan Plateau



Downloaded from http://pubs.geoscienceworld.org/gsa/geosphere/article-pdf/15/2/423/4663892/423.pdf
by guest

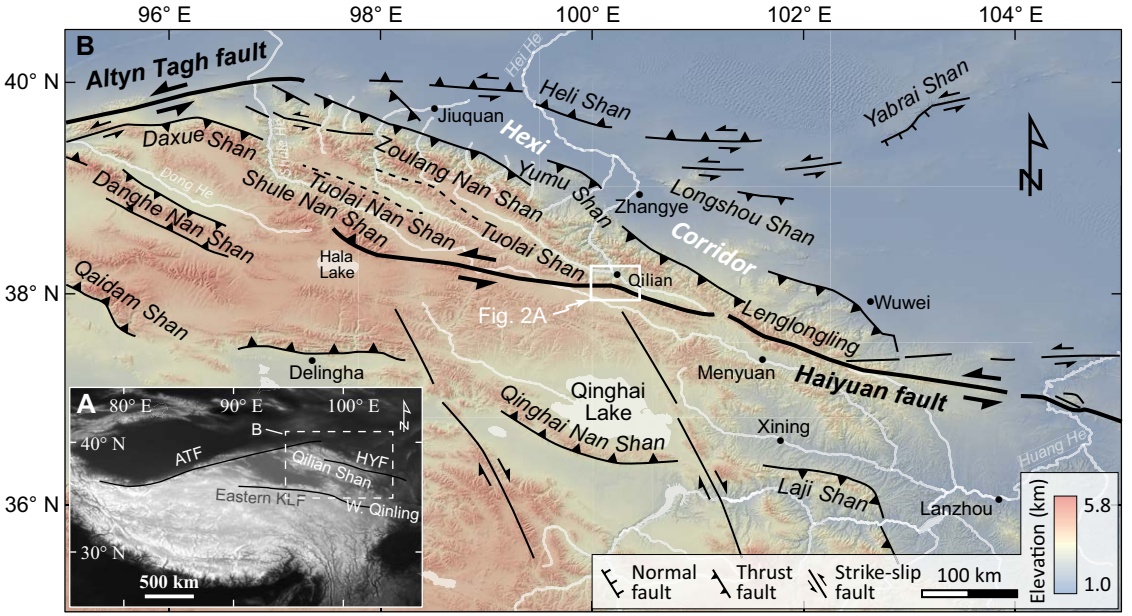


**Figure 1. (A) Map of the Tibetan Plateau and surrounding regions, showing the location of B. Abbreviations: ATF—Altyn Tagh fault; HYF—Haiyuan fault; Eastern KLF—Eastern Kunlun fault. (B) Topographic map of northern Tibet with active faults. Locations of active faults are from Yuan et al. (2013) and Yu et al. (2016).**

grew in a pulsed style, i.e., an Eocene outward expansion of crustal deformation with emergence of existing high terrain in the Miocene (Clark et al., 2010; Lease et al., 2012), or as a series of northward steps sequentially producing high topographic regions separated by basins (Meyer et al., 1998; Tapponnier et al., 2001).

To date, most thermochronologic data relevant to range uplift in northern Tibet were collected in the eastern Qilian Shan and the western Qinling range (e.g., Zheng et al., 2006; Clark et al., 2010; Duvall et al., 2011; Lease et al., 2011). In the inner and western Qilian Shan, these data indicate that the exhumation response to Cenozoic thrust and reverse faulting was insufficient to yield completely reset ages (George et al., 2001; Jolivet et al., 2001). The Qilian Shan is large, extending between the Qaidam Basin to the south and the Hexi Corridor to the north, entailing a width of ~300 km and length of >1000 km. It is entirely possible that it may have undergone initial deformation diachronously, and could also have experienced deformation styles during the Cenozoic that differ from those observed in the eastern Qilian Shan. Hence, more work on deformation timing and patterns in different parts of the Qilian Shan is required to understand the uplift and expansion mechanism of the Tibetan Plateau. In this paper, we present detailed apatite fission-track data from sites in the northern Qilian Shan showing that rapid cooling began between 17 and 15 Ma. Combining our apatite fission-track data with data from published studies of tectonic deformation in the northern Qilian Shan and Hexi Corridor, we discuss the deformation pattern in the northernmost part of the Tibetan Plateau.

## GEOLOGICAL SETTING

The WNW-trending Qilian Basin is a narrow intermontain basin with length of ~100 km and a width of <5 km. To the north, it is bounded by the Zoulang Nan Shan, which is mainly composed of metamorphic Paleozoic rocks that were thrusted in a northeastern direction over the Cenozoic sedimentary rocks in the Hexi Corridor (Gansu Geological Bureau, 1989). To the south the basin is bounded by the eastern Tuolai Shan, which is composed of folded late Paleozoic to early Mesozoic sediments and Precambrian metamorphic rocks (QBGMR, 1968). Rock units exposed in the Qilian Basin are dominated by Cretaceous conglomerate or sandstone and Quaternary alluvium, with sparse Neogene sandstone exposed (QBGMR, 1968). Using magnetostratigraphic and detrital fission-track data from the Qilian Basin, Liu et al. (2016) inferred that the conglomerate was deposited 14.3–10 Ma, which may suggest an increase in tectonic activity of the northern Qilian Shan at that time.

The ~1000-km-long Haiyuan strike-slip fault accommodates the eastward movement of Tibet relative to the Gobi Alashan block to the north (Fig. 1). Beginning east of Hala Lake, the 110°-striking Haiyuan fault can be traced eastward until its eastern termination near the Liupan Shan (Meyer et al., 1998; Yuan et al., 2013). Previous studies of the fault focused either on the slip rate (e.g., Lasserre et al., 1999, 2002; Li et al., 2009) or on the paleoseismology (e.g., Liu-Zeng et al., 2015; Ren et al., 2016) of the segments to the east of Lenglongling, which are characterized largely by left-lateral strike slip. Little work


Downloaded from http://pubs.geoscienceworld.org/gsa/geosphere/article-pdf/15/2/423/4663892/423.pdf
by guest

has focused on the western segments of the Haiyuan fault in the deep Qilian Shan because of remoteness and poorly preserved fault scarps in bedrock (Duvall et al., 2013). High-resolution satellite images and field investigations suggest that the Haiyuan fault extends across the Tuolai Shan south of Qilian town, and clear fault scarps and displaced left-lateral streams are preserved along the fault trace (Allen et al., 2017; Yuan D.Y., personal commun., 2017). Along the northern range front of the Tuolai Shan near the Qilian Basin, a thrust fault, the southern Qilian Basin fault, juxtaposes Precambrian metamorphic rocks over Cretaceous conglomerate or sandstone (QBGMR, 1968) (Fig. 2), although no evidence for late Quaternary activity along this fault has been found along the range front.

Because the Cenozoic sediments are distributed sparsely and thinly in the Qilian Basin, it is not easy to constrain the Cenozoic depositional history and evolution of the basin. Hence studying the uplift history of the mountain nearby is required in order to understand both the Cenozoic deformation around the Qilian Basin and its role in the deformation pattern of the northern margin of the Tibetan Plateau.

## APATITE FISSION-TRACK SAMPLING AND RESULTS

### Sampling Strategy and Data Measurement Procedures

Apatite fission-track (AFT) data provide information on the cooling path of thermochronology samples through the partial annealed zone (PAZ) at temperatures ranging from 60 to 110 ± 10 °C, corresponding to a depth of ~2–5 km (Laslett et al., 1987). Rapid-cooling events determined from AFT data are typically interpreted as the result of uplift and exhumation of rocks in response to

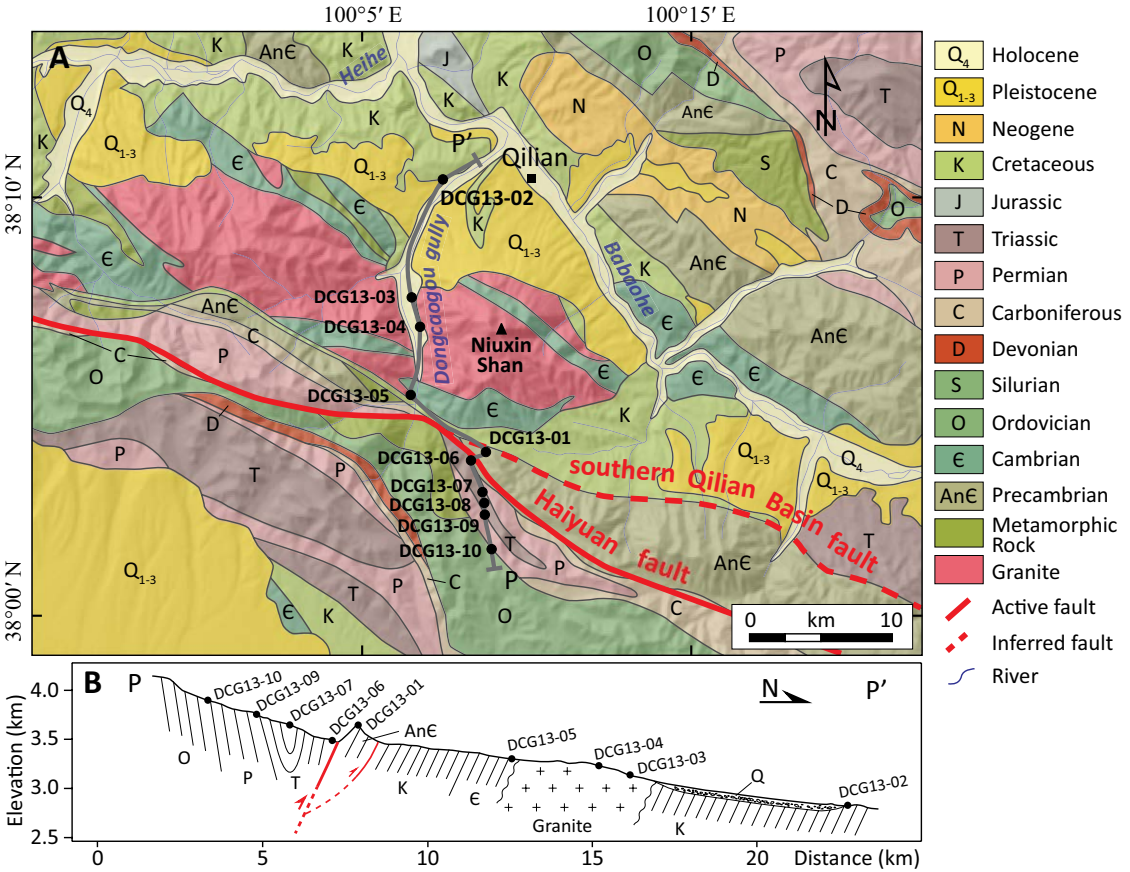


**Figure 2. Geological map of the Qilian Basin and its adjacent mountains (A) and geological cross section along profile P-P′ (B). Geological map is modified from QBGMR (1968). Red lines are major faults in the region: southern Qilian Basin fault and Haiyuan fault. Black dots are the locations of apatite fission-track samples.**


Downloaded from http://pubs.geoscienceworld.org/gsa/geosphere/article-pdf/15/2/423/4663892/423.pdf
by guest

dip-slip faulting (e.g., Green, 1988; Hendrix et al., 1994; Zheng et al., 2006) or to changes in erosion rates due to climatic variability (e.g., Molnar, 2003; Reiners et al., 2002). AFT thermochronology has been successfully used to date the onset of rapid cooling related to erosional exhumation in hanging-wall rocks (e.g., Hendrix et al., 1994; Zheng et al., 2006).

In order to delineate a cooling history of the Tuolai Shan, located to the south of the Qilian Basin, ten samples were collected for AFT dating along a tributary of Babaohe River, the Dongcaogou gully, situated southwest of Qilian town (Fig. 2A). Ten samples collected at ~100–200 m elevation intervals, covering a range of elevations from 2800 to 4100 m across the mountain. The units sampled are Cretaceous, Permian, Triassic, and Ordovician sandstones, Cambrian and Precambrian metamorphic rocks, and early Paleozoic granite (Fig. 2B). Four samples (DCG13-02, DCG13-03, DCG13-04, DCG13-05) were collected from the footwall of the southern Qilian Basin fault; sample DCG13-01 is from Precambrian bedrock between the southern Qilian Basin fault and the Haiyuan fault; and the other five samples (DCG13-06, DCG13-07, DCG13-08, DCG13-09, DCG13-10) were collected from folded Paleozoic bedrock south of the Haiyuan fault (Fig. 2).

More than 200 apatite crystals were picked for AFT dating except for sample DCG13-08. The AFT ages and track-length distribution were measured at the State Key Laboratory of Earthquake Dynamics, China Earthquake Administration, using the external detector method (Hurford and Green, 1983). A detailed description of the dating procedures can be found in Liu et al. (2013). The zeta ($\zeta$) value was calibrated to be 353 ± 10 using the Durango apatite and Fish Canyon Tuff international age standards. Samples were irradiated at the 492 Reactor, China Institute of Atomic Energy, and CN5 glass was irradiated at the same time to constrain the thermal-neutron flux received by the samples (Pang et al., 2013). To constrain the annealing kinetics of apatite, $D_{par}$ (diameter of etch figures parallel to the crystallographic *c*-axis) measurements were taken for all the grains for dating and track-length analysis (Donelick et al., 1999).

## Results

Dating results from the nine samples analyzed are listed in Table 1. They show central annealing ages ranging from 15.2 ± 0.8 to 53.8 ± 2.7 Ma. Confined mean track lengths are between 10.8 ± 1.35 and 13.3 ± 1.8 μm except for sample DCG13-01. Mean $D_{par}$ values are between 1.61 ± 0.2 and 2.33 ± 0.31 μm. Chi-squared ($\chi^2$) tests were performed for all the samples, and all but three relatively older samples (DCG13-02, DCG13-04, DCG13-05) passed the tests ($P[\chi^2] \geq 5\%$) (Fig. 3; Table 1).

The four lowest-elevation samples (DCG13-02, DCG13-03, DCG13-04, DCG13-05) have older annealing ages ranging from 42.4 ± 2.4 to 53.8 ± 2.7 Ma, which are significantly younger than the depositional and magmatic ages of the rocks (Cretaceous sandstone and early Paleozoic granite) (Figs. 2 and 3). Mean track lengths of these four samples range from 10.8 ± 1.35 to 11.5 ± 1.84 μm. Sample DCG13-01, collected between the Haiyuan fault and the

TABLE 1. DONGCAOGOU FISSION-TRACK AGE DATA

| Sample ID | Latitude (°E) | Longitude (°N) | Elevation (m) | $N_c$ | $\rho_d(N_d)$ ($\times10^6$ cm$^{-2}$) | $\rho_s(N_s)$ ($\times10^6$ cm$^{-2}$) | $\rho_i(N_i)$ ($\times10^6$ cm$^{-2}$) | U (ppm) | $P(\chi^2)$ % | Age ± 1σ (Ma) | ML ± 1σ (μm) ($N_l$) | $SD_{ML}$ (μm) | $D_{par}$ (μm) | $SD_{Dpar}$ (μm) |
|---|---|---|---|---|---|---|---|---|---|---|---|---|---|---|
| DCG13-01 | 100.231 | 38.065 | 3661 | 18 | 0.8688 (2172) | 0.1237 (149) | 0.7602 (916) | 9.81 | 12 | 25.7 ± 2.7 | NA | NA | 1.88 | 0.25 |
| DCG13-02 | 100.208 | 38.173 | 2814 | 30 | 0.876 (2190) | 0.3182 (41) | 1.1773 (2742) | 15.14 | 1 | 42.4 ± 2.4 | 11.5 ± 0.4 (18) | 1.84 | 1.92 | 0.45 |
| DCG13-03 | 100.191 | 38.125 | 3122 | 30 | 0.8833 (2208) | 0.8727 (2324) | 2.8607 (7618) | 37.37 | 24 | 47.4 ± 1.2 | 11.3 ± 0.1 (111) | 1.39 | 2.03 | 0.31 |
| DCG13-04 | 100.195 | 38.114 | 3222 | 30 | 0.8906 (2227) | 0.5841 (1313) | 2.1379 (4806) | 28.04 | 0 | 42.4 ± 1.9 | 11.4 ± 0.1 (67) | 1.19 | 2.33 | 0.31 |
| DCG13-05 | 100.194 | 38.088 | 3300 | 30 | 0.8979 (2245) | 0.4507 (1226) | 1.2971 (3528) | 16.67 | 0 | 53.8 ± 2.7 | 10.8 ± 0.2 (54) | 1.35 | 1.97 | 0.23 |
| DCG13-06 | 100.224 | 38.063 | 3470 | 17 | 0.9051 (2263) | 0.1503 (174) | 1.3653 (1581) | 17.53 | 84 | 17.6 ± 1.4 | 13 ± 0.4 (10) | 1.31 | 1.61 | 0.20 |
| DCG13-07 | 100.226 | 38.048 | 3661 | 30 | 0.9124 (2281) | 0.2289 (590) | 2.2387 (5769) | 29.33 | 10 | 16.1 ± 0.9 | 13.3 ± 0.4 (17) | 1.80 | 1.90 | 0.28 |
| DCG13-09 | 100.229 | 38.041 | 3724 | 30 | 0.9197 (2300) | 0.1753 (418) | 1.8704 (4459) | 23.55 | 99 | 15.2 ± 0.8 | 13.2 ± 0.7 (6) | 1.71 | 1.96 | 0.44 |
| DCG13-10 | 100.231 | 38.028 | 3883 | 30 | 0.927 (2318) | 0.1482 (237) | 0.7398 (1183) | 9.57 | 10 | 34.1 ± 2.9 | 12.1 ± 0.6 (7) | 1.59 | 2.19 | 0.41 |

*Notes:* $N_c$—number of apatite crystals analyzed; $\rho_d$—induced fission-track density calculated on muscovite external detectors used with $CN_5$ dosimeter; $N_d$—total number of fission tracks counted to determine $\rho_d$; $\rho_s$—spontaneous fission-track density on the internal surfaces of apatite crystals analyzed; $N_s$—total number of fission tracks counted to determine $\rho_s$; $\rho_i$—induced fission-track density on the muscovite external detector for crystals analyzed; $N_i$—total number of fission tracks counted to determine $\rho_i$; $P(\chi^2)$—chi-squared probability that all single-crystal ages represent a single population of ages where degrees of freedom = $N_c$-1 (Galbraith, 1981); ML—mean confined track length; $SD_{ML}$—standard deviation for ML; $N_l$—number of horizontally confined fission-track lengths measured; $D_{par}$—diameter of etch figures parallel to the crystallographic c-axis; $SD_{Dpar}$—standard deviation for $D_{par}$; U—K*U(glass)*($\rho_i/\rho_d$), in which K is from Jonckheere (2003); Apatite-$\zeta_{CN5}$ = 353.0 ± 10.



Downloaded from http://pubs.geoscienceworld.org/gsa/geosphere/article-pdf/15/2/423/4663892/423.pdf
by guest

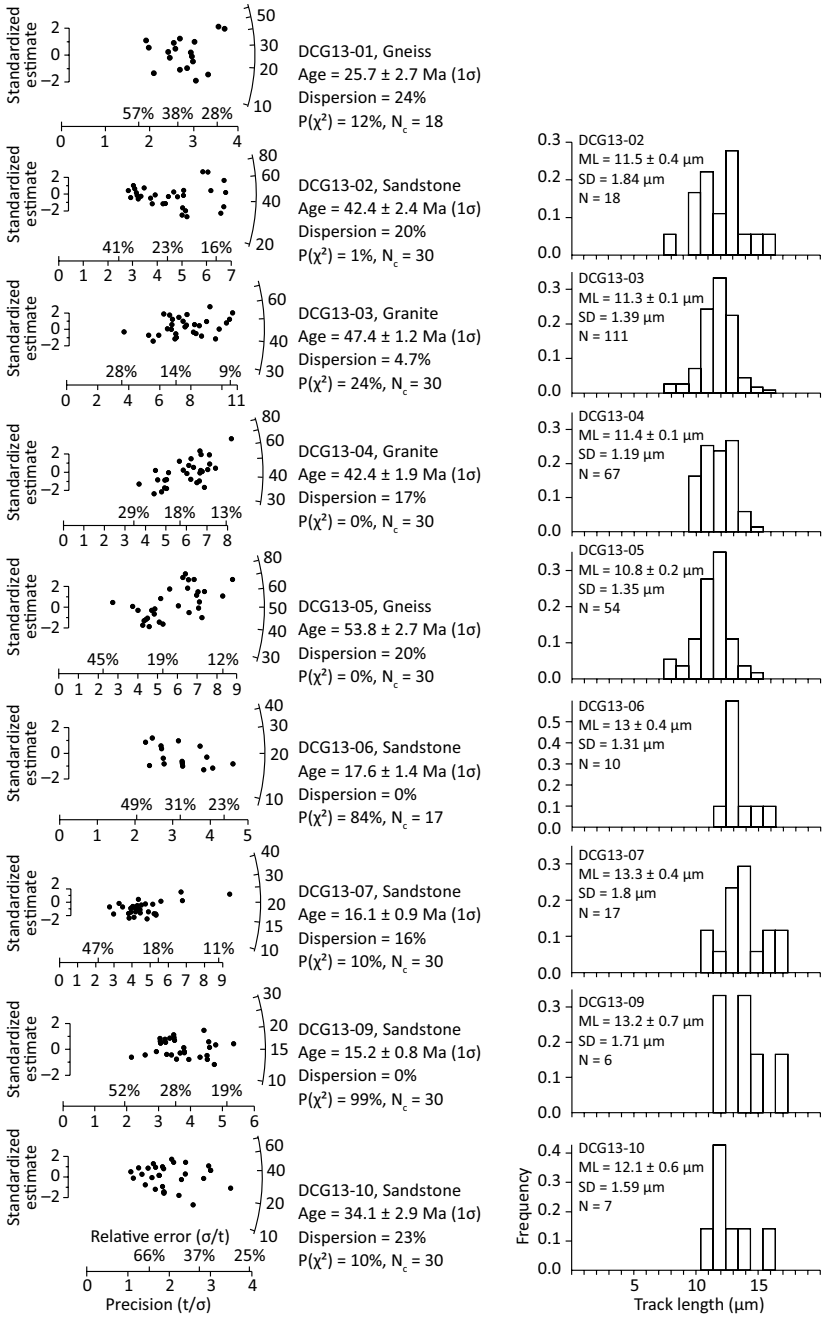


**Figure 3. Radial plots of fission-track ages and track-length histograms for the studied apatite samples. σ is the standard error and t is the single grain age. t/σ is the relative error. P($\chi^2$)—chi-squared probability is the probability of obtaining $\chi^2$ value for $N_c$-1 degrees of freedom (where $N_c$ is number of apatite crystals analyzed) (Galbraith, 1981); ML—mean confined track length; SD—standard deviation for ML. The track-length histogram of sample DCG13-01 is absent as few confined tracks were observed in the apatite crystals. Radial plots and histograms were constructed using RadialPlotter (Galbraith, 1990; Vermeesch, 2009).**

southern Qilian Basin fault, has an age of 25.7 ± 2.7 Ma, but was unfortunately without confined tracks measured in any grain (Fig. 3); therefore, we cannot determine the thermal history of this sample. To the south of the Haiyuan fault, three samples (DCG13-06, DCG13-07, DCG13-09) collected from late Paleozoic bedrock have mean fission-track ages ranging from 15.2 ± 0.8 to 17.6 ± 1.4 Ma (Figs. 2 and 3). Mean confined fission-track lengths are ≥13 μm. These three samples passed $\chi^2$ tests and radial plots show that grain ages are tightly clustered. Further to the south, the highest-elevation sample (DCG13-10) has an annealing age of 34.1 ± 2.9 Ma, younger than its depositional age (Permian), whereas its mean fission-track length of 12.1 ± 1.59 μm is shorter than that of the other three samples south of the Haiyuan fault (Fig. 3).

## DISCUSSION

### Constraint on the Onset of Deformation

Relatively older fission-track ages and shorter confined track lengths of the four lowest samples suggest that they experienced a long residence time in the PAZ. However, to the south of these four samples, sample DCG13-01 has higher elevation and much younger fission-track age, indicative of a more significant annealing. The differential annealing between sample DCG13-01 and the four lowest samples is apparently controlled by the southern Qilian Basin fault (Fig. 2). To the south of the Haiyuan fault, the three samples (DCG13-06, DCG13-07, DCG13-09) have tightly clustered middle Miocene ages (15.2 ± 0.8 to 17.6 ± 1.4 Ma) and relatively longer confined fission-track lengths (≥13 μm), suggesting that these three samples have been strongly annealed and that their fission-track ages have been reset. Compared to these three samples, the southernmost sample DCG13-10 has a relatively older fission-track age (34.1 ± 2.9 Ma) and a shorter confined fission-track length (12.1 ± 1.59 μm). It suggests that sample DCG13-10 has experienced a moderate degree of annealing.

The break in slope on AFT age-elevation and length-elevation plots is commonly interpreted to indicate the onset of rapid cooling due to denudation (Gallagher et al., 1998). The samples below the break have a consistently younger age and long mean fission-track length, suggesting that these samples rapidly passed though the PAZ, whereas the samples above the break, with older ages and shorter tracks, reflect a relatively long residence time in the PAZ and were partially annealed (Gleadow et al., 1986; Green et al., 1989). In the absence of thermal modeling, the relationship between fission-track ages of partially annealed samples and the timing of exhumation is unclear. On the AFT age-elevation and length-elevation plots of the samples from the Dongcaogou transect (Fig. 4), four samples (DCG13-02, DCG13-03, DCG13-04, DCG13-05) collected from the footwall of the southern Qilian Basin fault have relatively older fission-track ages that suggest a rough increase in age with increasing elevation. We interpret these samples as having undergone slow cooling within a Mesozoic to early Cenozoic PAZ (PAZ 1). However, four samples (DCG13-06, DCG13-07, DCG13-09, DCG13-10) collected from the hanging-


Downloaded from http://pubs.geoscienceworld.org/gsa/geosphere/article-pdf/15/2/423/4663892/423.pdf
by guest

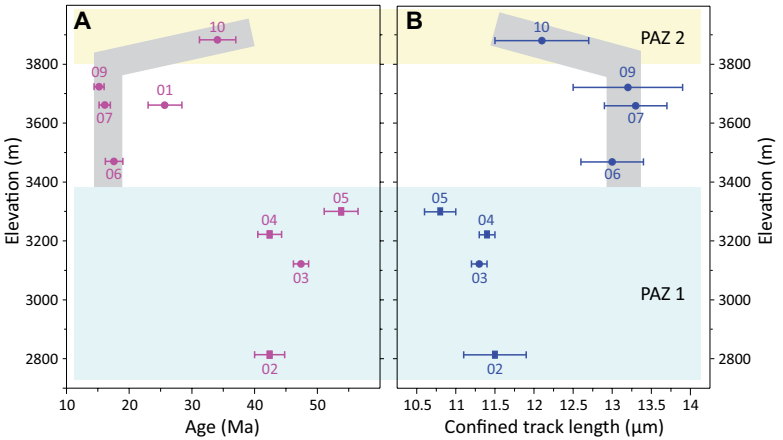


**Figure 4. Apatite fission-track (AFT) data from the Dongcaogou transect. (A) AFT age versus elevation plot. (B) Mean confined track length versus elevation. AFT age and track length are reported as central age with 1σ standard error and mean confined track length with 1σ standard error. Samples that passed $\chi^2$ test are marked as circles and those that do not pass the test are marked as rectangles. Light blue strip represents a partial annealing zone (PAZ 1) in the late Mesozoic to early Cenozoic, and the light yellow strip is interpreted as the Miocene partial annealing zone (PAZ 2). Grey strip is the inferred tendency of AFT ages and mean track lengths in the hanging wall of the Haiyuan fault.**

wall rocks of the Haiyuan fault have younger ages and show a sharp break in slope on AFT age-elevation and length-elevation plots (Fig. 4). Combining the different degrees of annealing and the small elevation separation (~160 m) between the samples DCG13-09 and DCG13-10, we infer that this break marks the base of an exhumed Miocene PAZ (PAZ 2) and defines the onset of a rapid cooling that occurred at ca. 17–15 Ma (Figs. 3 and 4).

## Exhumation and Cooling Due to Uplift of the Northern Qilian Shan

Apatite fission-track results from the Dongcaogou elevation transect show definitive accelerated cooling at 17–15 Ma. The three youngest samples (DCG13-06, DCG13-07, DCG13-09) of rocks exposed by exhumation appear to be local to the upthrown block of the Haiyuan fault rather than to be distributed on both sides. We attribute the rapid cooling to an increase in erosion rate following the initiation of the northward thrusting of the Haiyuan fault. Although it lacks measured confined tracks, sample DCG13-01, lying between the Haiyuan fault and the southern Qilian Basin fault, has a much younger age of 25.7 ± 2.7 Ma than the samples to the north. A single AFT age with no track length measurement does not provide any robust information about the cooling history, whereas sample DCG13-01, having passed the $\chi^2$ test, may suggest that its annealing age has been totally reset. If this is true, the southern Qilian Basin fault may have initiated earlier than the Haiyuan fault, which is consistent with observation of the activity of these two faults at present (Yuan D.Y., personal commun., 2017).

Two scenarios have been proposed to explain the timing of rapid uplift between 17–15 Ma along the Haiyuan fault. In scenario 1, the uplift is taken to constrain the timing of left-lateral slip along the western segment of the Haiyuan fault, which coincides very well with the results of thermochronology in the Dulan-Chaka highland to the south of the Tuolai Shan (Duvall et al., 2013). In the secondary scenario, the timing of 17–15 Ma is regarded as the time of initial northward thrust faulting along the Tuolai Shan, but not the initiation of left-lateral strike slip along the Haiyuan fault (e.g., Lease et al., 2011). Here, we prefer the second scenario for several reasons: (1) The Haiyuan fault is of limited extent, occupying only the ~100-km-long easternmost segment of the WNW-trending Tuolai Shan, which extends ~300–400 km in length from the eastern end of the Qilian Basin to the Changma Basin and is ~10–20 km wide (Fig. 1). In map view, the Tuolai Shan is just one of the WNW- to NW-trending elongated parallel mountain ranges in the northern eastern Tibetan Plateau, and these ranges are all bounded by active thrusts (Tapponnier et al., 1990; Meyer et al., 1998). (2) The Haiyuan fault extends across the Tuolai Shan to the south of Qilian town, cutting the Paleozoic to Mesozoic bedrock, although the total lateral strike slip is estimated to be only ~10 km (QBGMR, 1968; Allen et al., 2017). (3) Given rapid cooling ages observed in the Liupan Shan, a north-trending mountain range at the eastern end of the Haiyuan fault, Zheng et al. (2006) suggested that the onset of left-lateral strike slip on the Haiyuan fault was not earlier than 7.3–8.2 Ma. (4) Finally, the estimate placing the onset of left-lateral slip along the western segment of the Haiyuan fault at 17–12 Ma actually derives from rapid exhumation observed in the Dulan-Chaka highland (Duvall et al., 2013), which is located >100 km south of the Haiyuan fault. Combined with our data, these points suggest that the inner Qilian Shan experienced rapid exhumation in the mid-Miocene, and there is no evidence for left-lateral strike slip actually along the Haiyuan fault at that time.

Therefore, we infer that the rapid cooling of the Tuolai Shan in the middle Miocene was driven by an earlier phase of thrust – not left lateral strike-slip – activity on the Haiyuan fault, (termed here the ancestral Haiyuan thrust fault) along the Tuolai Shan range front. Then, induced by continued northward growth of the Tibetan Plateau, confined by the rigid Gobi Alashan block to the north (Dayem et al., 2009; Lease et al., 2011; Clark, 2012), the Miocene Haiyuan thrust connected with other faults in the northeastern plateau and finally formed the ~1000-km-long, active, left-lateral strike-slip Haiyuan fault in a later phase during the middle to late Miocene (Zhang et al., 1991; Zheng et al., 2006; Wang et al., 2013). This two-stage slip model of the Haiyuan fault zone coincides with the middle Miocene change in the kinematic style of plateau growth, from NNE-SSW contraction that mimicked the plate convergence direction to the inclusion of new structures accommodating east-west motion (Lease et al., 2011).

The 17–15 Ma timing of faulting found in this study agrees well with the increase in cooling rate and deposition throughout middle Miocene found in the Qilian Shan, Qaidam Basin, and Hexi Corridor (Fig. 5A). Evidence for the regional character of this change in tectonics includes: (1) the onset of motion on the western Haiyuan fault at 17–12 Ma from thermochronology results of three individual elevation transects (Duvall et al., 2013); (2) accelerated cooling


Downloaded from http://pubs.geoscienceworld.org/gsa/geosphere/article-pdf/15/2/423/4663892/423.pdf
by guest

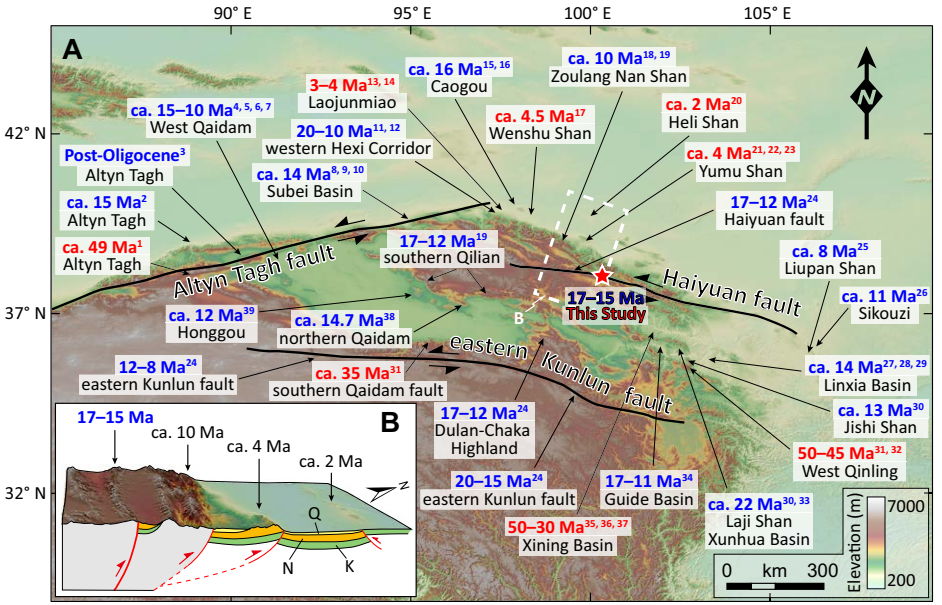


**Figure 5. (A) Timing of initial deformation across northern Tibet. Early to middle Miocene deformation timings are in blue. Initiation ages were derived from: 1—Yin et al. (2002); 2—Ritts et al. (2008); 3—Yue and Liou (1999); 4—Liu et al. (2017); 5—Chang et al. (2015); 6—Li et al. (2017); 7—Cheng et al. (2015); 8—Wang et al. (2003); 9—Sun et al. (2005); 10—Lin et al. (2015); 11—Bovet et al. (2009); 12—George et al. (2001); 13—Song et al. (2001); 14—Chen et al. (2006); 15—Wang et al. (2016a); 16—Wang et al. (2016b); 17—Zhao et al. (2001); 18—Zheng et al. (2010); 19—Zhuang et al. (2018); 20—Zheng et al. (2013); 21—Liu et al. (2011); 22—Palumbo et al. (2009); 23—Wang et al. (2018); 24—Duvall et al. (2013); 25—Zheng et al. (2006); 26—Wang et al. (2011); 27—Fang et al. (2003); 28—Garzione et al. (2005); 29—Hough et al. (2011); 30—Lease et al. (2011); 31—Clark et al. (2010); 32—Duvall et al. (2011); 33—Lease et al. (2012); 34—Yan et al. (2006); 35—Dupont-Nivet et al. (2004); 36—Horton et al. (2004); 37—Dai et al. (2006); 38—Fang et al. (2007); 39—Wang et al. (2017). (B) Schematic diagram showing a model of progressively northward growth in the northern margin of the Qilian Shan and Hexi Corridor. The four labeled ages from 17–15 to ca. 2 Ma refer to the timing of initial deformation in the Tuolai Shan (this study), Zoulang Nan Shan (Zheng et al., 2010; Zhuang et al., 2018), Yumu Shan (Palumbo et al., 2009; Liu et al., 2011; Wang et al., 2018), and Heli Shan (Zheng et al., 2013), respectively. K—Cretaceous sediments; N—Neogene sediments; Q—Quaternary alluvial and fluvial deposits.**

between ca. 20 and 10 Ma in the northern Qilian Shan revealed by AFT and (U-Th)/He thermochronology (George et al., 2001; Zhuang et al., 2018); (3) accelerated growth of the eastern Laji Shan at ca. 22 Ma, as indicated by apatite (U-Th)/He and AFT cooling ages (Lease et al., 2011); (4) emergence of the Jishi Shan between ca. 16 and 11 Ma, shown by stable isotope and thermochronologic evidence (Garzione et al., 2005; Hough et al., 2011; Lease et al., 2011); (5) rapid cooling of the northern margin of the Qilian Shan at ca. 10 Ma, indicated by apatite (U-Th)/He cooling ages (Zheng et al., 2010; Zhuang et al., 2018); (6) a greatly reduced slip rate in the early mid-Miocene along the Altyn Tagh fault (Yue and Liou, 1999); (7) initiation of deposition or provenance change in the Hexi Corridor in the middle Miocene (Bovet et al., 2009; Wang et al., 2016a, 2016b); (8) initiation of Tertiary sedimentation in the Qilian Basin at ca. 14.3 Ma (Liu et al., 2016); (9) rapid exhumation and increasing deposition rates at ca. 15 Ma in the southern Qilian Shan and northern Qaidam Basin (Fang et al., 2007; Wang et al., 2017; Zhuang et al., 2018); and (10) growth strata starting to develop at ca. 15–10 Ma in the western Qaidam Basin (Chang et al., 2015; Cheng et al., 2015; Li et al., 2017; Liu et al., 2017). These temporally proximate processes indicate that the Qilian Shan experienced synchronous deformation in the middle Miocene.

## Northward Growth of the Northern Margin of the Qilian Shan

Synthesis of new AFT data from this study with published constraints on the timing of initial deformation within the northern Qilian Shan and Hexi Corridor allows us to explore the late Cenozoic deformation pattern of the region. We propose a north-northeastward progressive deformation pattern for the northernmost part of the Qilian Shan and Hexi Corridor from the Miocene to the Quaternary (Fig. 5B).

Northern Tibet, bounded by the Kunlun, Altyn Tagh, and Haiyuan fault systems, has been regarded as the Plio-Quaternary Tibet (Tapponnier et al., 2001). Northern Tibet consists of several parallel mountain ranges that are separated by subparallel intermontain basins (Fig. 1). In the last decade, many studies have examined the onset of rapid uplift of these mountain ranges and the depositional histories of the intermontain basins, allowing us to build a deformation sequence for northern Tibet (Fig. 5). Prior to the Miocene, northern Tibet appears to have undergone contractional deformation and surface uplift ca. 45–50 Ma, beginning roughly near the onset of India-Eurasia collision (e.g., Jolivet et al., 2001; Yin et al., 2002, 2008; Horton et al., 2004; Dupont-Nivet et al., 2004; Clark et al., 2010; Duvall et al., 2011). Evidence for deformation since the Miocene is distributed across northern Tibet (e.g., George et al., 2001; Fang et al., 2003; Palumbo et al., 2009; Zheng et al., 2006, 2010; Lease et al., 2011, 2012; Yuan et al., 2013; Wang et al., 2011, 2016a, 2016b; Zhuang et al., 2018).

Focusing on the timing of initial deformation in the northern margin of the Qilian Shan and Hexi Corridor, we find that a progressive northward growth model since the early to middle Miocene is suitable (Fig. 5B). Lease et al. (2011) reported an accelerated growth of the WNW-trending Laji Shan that began at ca. 22 Ma, constrained by AFT thermochronology. The Dulan-Chaka highland to the south of the Tuolai Shan is supposed to have rapidly uplifted by


Downloaded from http://pubs.geoscienceworld.org/gsa/geosphere/article-pdf/15/2/423/4663892/423.pdf
by guest

ca. 17–12 Ma (Duvall et al., 2011). Our AFT data from the Tuolai Shan suggest rapid cooling at 17–15 Ma, which we interpret to represent the onset of northward thrust faulting along the Haiyuan fault. For the region further to the north, Zheng et al. (2010) suggested that rapid cooling of the northern margin of the Qilian Shan that started at ca. 10 Ma, as determined by (U-Th)/He thermochronology, resulted from northward thrusting of the northern Qilian fault. Growth of the Yumu Shan, a high mountain north of the Qilian Shan, is thought to have started ~4 m.y. ago (Palumbo et al., 2009; Liu et al., 2011; Wang et al., 2018). Similarly, magnetostratigraphic analysis results suggest that the Wenshu Shan and Laojunmiao anticline, two other relatively low topographic ramp anticlines in the western Hexi Corridor, started to uplift at ca. 4.5–3 Ma (Zhao et al., 2001; Song et al., 2001; Fang et al., 2005; Chen et al., 2006; Zheng et al., 2017). To the north of the Hexi Corridor, a series of low-relief north-dipping thrust ramps lying parallel to the Qilian Shan range front are thought to have been active since the Quaternary (Zheng et al., 2013).

Therefore, we suggest that the northernmost Qilian Shan has grown north-northeastward toward the foreland since the Miocene to create a series of parallel WNW-striking ramp anticlines and associated NNE–striking thrust faults. Foreland basins formed along the range fronts as the mountains uplifted, which then evolved into piggyback basins when the ranges to the north of these basins began to uplift, and finally became the subparallel elongated intermountain basins. As seen today, the Hexi Corridor, as the foreland basin of the northern Qilian Shan at the present time, is evolving into a piggyback basin as the ranges to the north are uplifting. Widespread middle Miocene deformation, as indicated by accelerated erosion and deposition not only in the northern Qilian Shan, but also in the southern Qilian Shan (Zhuang et al., 2018), northern Qaidam Basin (Fang et al., 2007; Wang et al., 2017), and western Qaidam Basin (e.g., Chang et al., 2015; Cheng et al., 2015; Li et al., 2017; Liu et al., 2017), may therefore be inconsistent with a simple model of northward growth for northern Tibet. Widespread middle Miocene deformation across northern Tibet is consistent with the predicted timing of initial rapid outward growth driven by removal of mantle lithosphere from beneath Tibet (England and Houseman, 1989; Molnar and Stock, 2009).

## CONCLUSIONS

This work provides new constraints on the onset of rapid cooling in northern Tibet by AFT thermochronometry in samples collected from the Tuolai Shan, one of the WNW- to NW-trending elongated mountain ranges in the Qilian Shan. The break in slope on AFT age-elevation and length-elevation plots provides a definitive tie to an initial deformation that occurred at 17–15 Ma. We interpret this rapid cooling to indicate that northward thrusting occurred on an ancestral Haiyuan fault along the Tuolai Shan range front. Correlating accelerated thrust activity with initial deformation in the north Qilian Shan and Hexi Corridor, we propose a north-northeastward progressive growth model for the northernmost part of the Tibetan Plateau.

### ACKNOWLEDGMENTS

This work was supported by the Fundamental Scientific Research of the Institute of Geology, China Earthquake Administration (IGCEA1509), the National Science Foundation of China (41474053, 41603054, 41622204, 41761144071), and the UK Natural Environment Research Council (NERC) through the Seismicity and Tectonics in Ninxia, Gansu, and Sha'anxi (STINGS) project (NE/N012313/1). We gratefully acknowledge Richard T. Walker and Peter Molnar for their comments on this paper. We thank Mark B. Allen, an anonymous reviewer, and the science editor Raymond M. Russo for constructive reviews.

### REFERENCES CITED

Allen, M.B., Walters, R.J., Song, S., Saville, C., De Paola, N., Ford, J., Hu, Z., and Sun, W., 2017, Partitioning of oblique convergence coupled to the fault locking behavior of fold-and-thrust belts: Evidence from the Qilian Shan, northeastern Tibetan Plateau: Tectonics, v. 36, p. 1679–1698, https://doi.org/10.1002/2017TC004476.

Bovet, P.M., Ritts, B.D., Gehrels, G., Abbink, A.O., Darby, B., and Hourigan, J., 2009, Evidence of Miocene crustal shortening in the north Qilian Shan from Cenozoic stratigraphy of the western Hexi Corridor, Gansu Province, China: American Journal of Science, v. 309, p. 290–329, https://doi.org/10.2475/00.4009.02.

Burchfiel, B.C., Deng, Q., Molnar, P., Royden, L., Wang, Y., Zhang, P., and Zhang, W., 1989, Intracrustal detachment within zones of continental deformation: Geology, v. 17, p. 748–752, https://doi.org/10.1130/0091-7613(1989)017<0448:IDWZOC>2.3.CO;2.

Chang, H., Li, L., Qiang, X., Garzione, C.N., Pullen, A., and An, Z., 2015, Magnetostratigraphy of Cenozoic deposits in the western Qaidam Basin and its implication for the surface uplift of the northeastern margin of the Tibetan Plateau: Earth and Planetary Science Letters, v. 430, p. 271–283, https://doi.org/10.1016/j.epsl.2015.08.029.

Chen, J., Wyrwoll, K.-H., Lu, Y., Krapez, B., Wan, J., and Liu, J., 2006, Magnetochronology of the Yumen conglomerates and multi-pulsed folding and thrusting in the northern Qilianshan: Quaternary Sciences, v. 26, p. 20–31 (in Chinese).

Cheng, F., Guo, Z., Jenkins, H.S., Fu, S., and Cheng, X., 2015, Initial rupture and displacement on the Altyn Tagh fault, northern Tibetan Plateau: Constraints based on residual Mesozoic to Cenozoic strata in the western Qaidam Basin: Geosphere, v. 11, p. 921–942, https://doi.org/10.1130/GES01070.1.

Clark, M.K., 2012, Continental collision slowing due to viscous mantle lithosphere rather than topography: Nature, v. 483, p. 74–77, https://doi.org/10.1038/nature10848.

Clark, M.K., Farley, K.A., Zheng, D., Wang, Z., and Duvall, A.R., 2010, Early Cenozoic faulting of the northern Tibetan Plateau margin from apatite (U-Th)/He ages: Earth and Planetary Science Letters, v. 296, p. 78–88, https://doi.org/10.1016/j.epsl.2010.04.051.

Dai, S., Fang, X.M., Dupont-Nivet, G., Song, C., Gao, J., Krijgsman, W., Langereis, C., and Zhang, W., 2006, Magnetostratigraphy of Cenozoic sediments from the Xining Basin: Tectonic implications for the northeastern Tibetan Plateau: Journal of Geophysical Research, v. 111, B11102, https://doi.org/10.1029/2005JB004187.

Dayem, K.E., Molnar, P., Clark, M.K., and Houseman, G.A., 2009, Far-field lithospheric deformation in Tibet during continental collision: Tectonics, v. 28, TC6005, https://doi.org/10.1029/2008TC002344.

Donelick, R.A., Ketcham, R.A., and Carlson, W.D., 1999, Variability of apatite fission-track annealing kinetics: II. Crystallographic orientation effects: The American Mineralogist, v. 84, p. 1224–1234, https://doi.org/10.2138/am-1999-0902.

Dupont-Nivet, G., Horton, B.K., Butler, R.F., Wang, J., Zhou, J., and Waanders, G.L., 2004, Paleogene clockwise tectonic rotation of the Xining-Lanzhou region, northeastern Tibetan Plateau: Journal of Geophysical Research, v. 109, B04401, https://doi.org/10.1029/2003JB002620.

Duvall, A.R., Clark, M.K., van der Pluijm, B.A., and Li, C., 2011, Direct dating of Eocene reverse faulting in northeastern Tibet using Ar-dating of fault clays and low-temperature thermochronometry: Earth and Planetary Science Letters, v. 304, p. 520–526, https://doi.org/10.1016/j.epsl.2011.02.028.

Duvall, A.R., Clark, M.K., Kirby, E., Farley, K.A., Craddock, W.H., Li, C., and Yuan, D.Y., 2013, Low-temperature thermochronometry along the Kunlun and Haiyuan Faults, NE Tibetan Plateau: Evidence for kinematic change during late-stage orogenesis: Tectonics, v. 32, p. 1190–1211, https://doi.org/10.1002/tect.20072.



Downloaded from http://pubs.geoscienceworld.org/gsa/geosphere/article-pdf/15/2/423/4663892/423.pdf
by guest

England, P., and Houseman, G., 1986, Finite strain calculations of continental deformation: 2. Comparison with the India-Asia collision zone: Journal of Geophysical Research, v. 91, p. 3664–3676, https://doi.org/10.1029/JB091iB03p03664.

England, P., and Houseman, G., 1989, Extension during continental convergence, with application to the Tibetan Plateau: Journal of Geophysical Research, v. 94, p. 17,561–17,579, https://doi.org/10.1029/JB094iB12p17561.

Fang, X., Garzione, C., Van der Voo, R., Li, J., and Fan, M., 2003, Flexural subsidence by 29 Ma on the NE edge of Tibet from the magnetostratigraphy of Linxia Basin, China: Earth and Planetary Science Letters, v. 210, p. 545–560, https://doi.org/10.1016/S0012-821X(03)00142-0.

Fang, X., Zhao, Z., Li, J., Yan, M.D., Pan, B.T., Song, C.H., and Dai, S., 2005, Magnetostratigraphy of the late Cenozoic Laojunmiao anticline in the northern Qilian Mountains and its implications for the northern Tibetan Plateau uplift: Science in China, Series D: Earth Sciences, v. 48, p. 1040–1051, https://doi.org/10.1360/03yd0188.

Fang, X., Zhang, W., Meng, Q., Gao, J., Wang, X., King, J., Song, C., Dai, S., and Miao, Y., 2007, High-resolution magnetostratigraphy of the Neogene Huaitoutala section in the eastern Qaidam Basin on the NE Tibetan Plateau, Qinghai Province, China and its implication on tectonic uplift of the NE Tibetan Plateau: Earth and Planetary Science Letters, v. 258, p. 293–306, https://doi.org/10.1016/j.epsl.2007.03.042.

Galbraith, R.F., 1981, On statistical models for fission track counts: Mathematical Geology, v. 13, p. 471–478, https://doi.org/10.1007/BF01034498.

Galbraith, R.F., 1990, The radial plot: Graphical assessment of spread in ages: Nuclear Tracks and Radiation Measurements, v. 17, p. 207–214, https://doi.org/10.1016/1359-0189(90)90036-W.

Gallagher, K., Brown, R., and Johnson, C., 1998, Fission track analysis and its applications to geological problems: Annual Review of Earth and Planetary Sciences, v. 26, p. 519–572, https://doi.org/10.1146/annurev.earth.26.1.519.

Gansu Geological Bureau, 1989, Regional Geology of Gansu Province: Beijing, Geological Publishing House, 692 p. (in Chinese).

Garzione, C.N., Ikari, M.J., and Basu, A.R., 2005, Source of Oligocene to Pliocene sedimentary rocks in the Linxia basin in northeastern Tibet from Nd isotopes: Implications for tectonic forcing of climate: Geological Society of America Bulletin, v. 117, p. 1156–1166, https://doi.org/10.1130/B25743.1.

George, A.D., Marshallsea, S.J., Wyrwoll, K.-H., Chen, J., and Lu, Y., 2001, Miocene cooling in the northern Qilian Shan, northeastern margin of the Tibetan Plateau, revealed by apatite fission-track and vitrinite-reflectance analysis: Geology, v. 29, p. 939–942, https://doi.org/10.1130/0091-7613(2001)029<0939:MCITNQ>2.0.CO;2.

Gleadow, A.J.W., Duddy, I.R., Green, P.F., and Lovering, J.F., 1986, Confined fission track lengths in apatite: A diagnostic tool for thermal history analysis: Contributions to Mineralogy and Petrology, v. 94, p. 405–415, https://doi.org/10.1007/BF00376334.

Green, P.F., 1988, The relationship between track shortening and fission track age reduction in apatite: Combined influences of inherent instability, annealing anisotropy, length bias and system calibration: Earth and Planetary Science Letters, v. 89, p. 335–352, https://doi.org/10.1016/0012-821X(88)90121-5.

Green, P.F., Duddy, I.R., Gleadow, A.J., and Lovering, J.F., 1989, Apatite fission-track analysis as a paleotemperature indicator for hydrocarbon exploration, *in* Naeser, N.D., and McCulloh, T.H., eds., Thermal History of Sedimentary Basins: Methods and Case Histories: New York, Springer, p. 181–195, https://doi.org/10.1007/978-1-4612-3492-0_11.

Hendrix, M.S., Dumitru, T.A., and Graham, S.A., 1994, Late Oligocene–early Miocene unroofing in the Chinese Tian Shan: An early effect of the India-Asia collision: Geology, v. 22, p. 487–490, https://doi.org/10.1130/0091-7613(1994)022<0487:LOEMUI>2.3.CO;2.

Horton, B.K., Dupont-Nivet, G., Zhou, J., Waanders, G.L., Butler, R.F., and Wang, J., 2004, Mesozoic-Cenozoic evolution of the Xining-Minhe and Dangchang basins, northeastern Tibetan Plateau: Magnetostratigraphic and biostratigraphic results: Journal of Geophysical Research, v. 109, no. B4, https://doi.org/10.1029/2003JB002913.

Hough, B.G., Garzione, C.N., Wang, Z., Lease, R.O., Burbank, D.W., and Yuan, D., 2011, Stable isotope evidence for topographic growth and basin segmentation: Implications for the evolution of the NE Tibetan Plateau: Geological Society of America Bulletin, v. 123, p. 168–185, https://doi.org/10.1130/B30090.1.

Hurford, A.J., and Green, P.F., 1983, The zeta age calibration of fission-track dating: Chemical Geology, v. 41, p. 285–317, https://doi.org/10.1016/S0009-2541(83)80026-6.

Jolivet, M., Brunel, M., Seward, D., Xu, Z., Yang, J., Roger, F., Tapponnier, P., Malavieille, J., Arnaud, N., and Wu, C., 2001, Mesozoic and Cenozoic tectonics of the northern edge of the Tibetan plateau: Fission-track constraints: Tectonophysics, v. 343, p. 111–134, https://doi.org/10.1016/S0040-1951(01)00196-2.

Jonckheere, R., 2003, On the densities of etchable fission tracks in a mineral and co-irradiated external detector with reference to fission-track dating of minerals: Chemical Geology, v. 200, p. 41–58, https://doi.org/10.1016/S0009-2541(03)00116-5.

Laslett, G.M., Green, P.F., Duddy, I.R., and Gleadow, A.J.W., 1987, Thermal annealing of fission tracks in apatite 2. A quantitative analysis: Chemical Geology: Isotope Geoscience Section, v. 65, p. 1–13, https://doi.org/10.1016/0168-9622(87)90057-1.

Lasserre, C., Morel, P.-H., Gaudemer, Y., Tapponnier, P., Ryerson, F.J., King, G.C.P., Métivier, F., Kasser, M., Kashgarian, M., and Liu, B., 1999, Postglacial left slip rate and past occurrence of $M \geq 8$ earthquakes on the western Haiyuan fault, Gansu, China: Journal of Geophysical Research, v. 104, p. 17,633–17,651, https://doi.org/10.1029/1998JB900082.

Lasserre, C., Gaudemer, Y., Tapponnier, P., Mériaux, A.-S., Van der Woerd, J., Daoyang, Y., Ryerson, F.J., Finkel, R.C., and Caffee, M.W., 2002, Fast late Pleistocene slip rate on the Leng Long Ling segment of the Haiyuan fault, Qinghai, China: Journal of Geophysical Research, v. 107, 2276, https://doi.org/10.1029/2000JB000060.

Lease, R.O., Burbank, D.W., Clark, M.K., Farley, K.A., Zheng, D., and Zhang, H., 2011, Middle Miocene reorganization of deformation along the northeastern Tibetan Plateau: Geology, v. 39, p. 359–362, https://doi.org/10.1130/G31356.1.

Lease, R.O., Burbank, D.W., Hough, B., Wang, Z., and Yuan, D., 2012, Pulsed Miocene range growth in northeastern Tibet: Insights from Xunhua Basin magnetostratigraphy and provenance: Geological Society of America Bulletin, v. 124, p. 657–677, https://doi.org/10.1130/B30524.1.

Li, B., Yan, M., Zhang, W., Fang, X., Meng, Q., Zan, J., Chen, Y., Zhang, D., Yang, Y., and Guan, C., 2017, New paleomagnetic constraints on middle Miocene strike-slip faulting along the middle Altyn Tagh Fault: Journal of Geophysical Research: Solid Earth, v. 122, p. 4106–4122, https://doi.org/10.1002/2017JB014058.

Li, C., Zhang, P., Yin, J., and Min, W., 2009, Late Quaternary left-lateral slip rate of the Haiyuan fault, northeastern margin of the Tibetan Plateau: Tectonics, v. 28, TC5010, https://doi.org/10.1029/2008TC002302.

Lin, X., Zheng, D., Sun, J., Windley, B.F., Tian, Z., Gong, Z., and Jia, Y., 2015, Detrital apatite fission track evidence for provenance change in the Subei Basin and implications for the tectonic uplift of the Danghe Nan Shan (NW China) since the mid-Miocene: Journal of Asian Earth Sciences, v. 111, p. 302–311, https://doi.org/10.1016/j.jseaes.2015.07.007.

Liu, C., Wang, W., Zhang, P., Pang, J., and Yu, J., 2016, Magnetostratigraphy and magnetic anisotropy of the Neogene sediments in the Qilian Basin: Chinese Journal of Geophysics (Chinese edition), v. 59, p. 2965–2978, https://doi.org/10.6038/cjg20160820.

Liu, D., Yan, M., Fang, X., Li, H., Song, C., and Dai, S., 2011, Magnetostratigraphy of sediments from the Yumu Shan, Hexi Corridor and its implications regarding the Late Cenozoic uplift of the NE Tibetan Plateau: Quaternary International, v. 236, p. 13–20, https://doi.org/10.1016/j.quaint.2010.12.007.

Liu, J., Zhang, P., Lease, R.O., Zheng, D., Wan, J., Wang, W., and Zhang, H., 2013, Eocene onset and late Miocene acceleration of Cenozoic intracontinental extension in the North Qinling range–Weihe graben: Insights from apatite fission track thermochronology: Tectonophysics, v. 584, p. 281–296, https://doi.org/10.1016/j.tecto.2012.01.025.

Liu, R., Allen, M.B., Zhang, Q., Du, W., Cheng, X., Holdsworth, R.E., and Guo, Z., 2017, Basement controls on deformation during oblique convergence: Transpressive structures in the western Qaidam Basin, northern Tibetan Plateau: Lithosphere, v. 9, p. 583–594, https://doi.org/10.1130/L634.1.

Liu-Zeng, J., Shao, Y., Klinger, Y., Xie, K., Yuan, D., and Lei, Z., 2015, Variability in magnitude of paleoearthquakes revealed by trenching and historical records, along the Haiyuan Fault, China: Journal of Geophysical Research: Solid Earth, v. 120, p. 8304–8333, https://doi.org/10.1002/2015JB012163.

Meyer, B., Tapponnier, P., Bourjot, L., Métivier, F., Gaudemer, Y., Peltzer, G., Guo, S., and Chen, Z., 1998, Crustal thickening in Gansu-Qinghai, lithospheric mantle subduction, and oblique, strike-slip controlled growth of the Tibet plateau: Geophysical Journal International, v. 135, p. 1–47, https://doi.org/10.1046/j.1365-246X.1998.00567.x.

Molnar, P., 2003, Geomorphology: Nature, nurture and landscape: Nature, v. 426, p. 612–614, https://doi.org/10.1038/426612a.

Molnar, P., and Stock, J.M., 2009, Slowing of India's convergence with Eurasia since 20 Ma and its implications for Tibetan mantle dynamics: Tectonics, v. 28, TC3001, https://doi.org/10.1029/2008TC002271.



Downloaded from http://pubs.geoscienceworld.org/gsa/geosphere/article-pdf/15/2/423/4663892/423.pdf
by guest

Molnar, P., and Tapponnier, P., 1975, Cenozoic tectonics of Asia: Effects of a continental collision: Science, v. 189, p. 419–426, https://doi.org/10.1126/science.189.4201.419.

Palumbo, L., Hetzel, R., Tao, M., Li, X., and Guo, J., 2009, Deciphering the rate of mountain growth during topographic presteady state: An example from the NE margin of the Tibetan Plateau: Tectonics, v. 28, TC4017, https://doi.org/10.1029/2009TC002455.

Pang, J., Zheng, D., Wan, J., Li, D., Zhang, P., and Yang, J., 2013, Insufficient thermalization effects on determining fission-track ages: Science China Earth Sciences, v. 56, p. 1233–1241, https://doi.org/10.1007/s11430-012-4471-7.

Qinghai Bureau of Geology and Mineral Resources (QBGMR), 1968, 1:200,000 scale geologic and mineral resources map of the Qilian sheet (in Chinese): Beijing, Geological Publishing House.

Reiners, P.W., Ehlers, T.A., Garver, J.I., Mitchell, S.G., Montgomery, D.R., Vance, J.A., and Nicolescu, S., 2002, Late Miocene exhumation and uplift of the Washington Cascade Range: Geology, v. 30, p. 767–770, https://doi.org/10.1130/0091-7613(2002)030<0767:LMEAUO>2.0.CO;2.

Ren, Z., Zhang, Z., Chen, T., Yan, S., Yin, J., Zhang, P., Zheng, W., Zhang, H., and Li, C., 2016, Clustering of offsets on the Haiyuan fault and their relationship to paleoearthquakes: Geological Society of America Bulletin, v. 128, p. 3–18, https://doi.org/10.1130/B31155.1.

Ritts, B.D., Yue, Y., Graham, S.A., Sobel, E.R., Abbink, O.A., and Stockli, D., 2008, From sea level to high elevation in 15 million years: Uplift history of the northern Tibetan Plateau margin in the Altun Shan: American Journal of Science, v. 308, p. 657–678, https://doi.org/10.2475/05.2008.01.

Royden, L.H., Burchfiel, B.C., and van der Hilst, R.D., 2008, The geological evolution of the Tibetan Plateau: Science, v. 321, p. 1054–1058, https://doi.org/10.1126/science.1155371.

Song, C., Fang, X., Li, J., Gao, J., Zhao, Z., and Fan, M., 2001, Tectonic uplift and sedimentary evolution of the Jiuxi Basin in the northern margin of the Tibetan Plateau since 13 Ma BP: Science in China, Series D: Earth Sciences, v. 44, p. 192–202, https://doi.org/10.1007/BF02911987.

Sun, J., Zhu, R., and An, Z., 2005, Tectonic uplift in the northern Tibetan Plateau since 13.7 Ma ago inferred from molasse deposits along the Altyn Tagh Fault: Earth and Planetary Science Letters, v. 235, p. 641–653, https://doi.org/10.1016/j.epsl.2005.04.034.

Tapponnier, P., and Molnar, P., 1979, Active faulting and Cenozoic tectonics of the Tien Shan, Mongolia, and Baykal regions: Journal of Geophysical Research, v. 84, p. 3425–3459, https://doi.org/10.1029/JB084iB07p03425.

Tapponnier, P., Meyer, B., Avouac, J.P., Peltzer, G., Gaudemer, Y., Guo, S., Xiang, H., Yin, K., Chen, Z., Cai, S., and Dai, H., 1990, Active thrusting and folding in the Qilian Shan, and decoupling between upper crust and mantle in northeastern Tibet: Earth and Planetary Science Letters, v. 97, p. 382–383, 387–403, https://doi.org/10.1016/0012-821X(90)90053-Z.

Tapponnier, P., Xu, Z., Roger, F., Meyer, B., Arnaud, N., Wittlinger, G., and Yang, J., 2001, Oblique stepwise rise and growth of the Tibet plateau: Science, v. 294, p. 1671–1677, https://doi.org/10.1126/science.105978.

Vermeesch, P., 2009, RadialPlotter: A Java application for fission track, luminescence and other radial plots: Radiation Measurements, v. 44, p. 409–410, https://doi.org/10.1016/j.radmeas.2009.05.003.

Wang, W., Zhang, P., Kirby, E., Wang, L., Zhang, G., Zheng, D., and Chai, C., 2011, A revised chronology for Tertiary sedimentation in the Sikouzi basin: Implications for the tectonic evolution of the northeastern corner of the Tibetan Plateau: Tectonophysics, v. 505, p. 100–114, https://doi.org/10.1016/j.tecto.2011.04.006.

Wang, W., Kirby, E., Zhang, P., Zheng, D., Zhang, G., Zhang, H., Zheng, W., and Chai, Z., 2013, Tertiary basin evolution along the northeastern margin of the Tibetan Plateau: Evidence for basin formation during Oligocene transtension: Geological Society of America Bulletin, v. 125, p. 377–400, https://doi.org/10.1130/B30611.1.

Wang, W., Zhang, P., Pang, J., Garzione, C., Zhang, H., Liu, C., Zheng, D., Zheng, W., and Yu, J., 2016a, The Cenozoic growth of the Qilian Shan in the northeastern Tibetan Plateau: A sedimentary archive from the Jiuxi Basin: Journal of Geophysical Research: Solid Earth, v. 121, p. 2235–2257, https://doi.org/10.1002/2015JB012689.

Wang, W., Zhang, P., Yu, J., Wang, Y., Zheng, D., Zheng, W., Zhang, H., and Pang, J., 2016b, Constraints on mountain building in the northeastern Tibet: Detrital zircon records from synorogenic deposits in the Yumen Basin: Scientific Reports, v. 6, 27604, https://doi.org/10.1038/srep27604.

Wang, W., Zheng, W., Zhang, P., Li, Q., Kirby, E., Yuan, D., Zheng, D., Liu, C., Wang, Z., Zhang, H., and Pang, J., 2017, Expansion of the Tibetan Plateau during the Neogene: Nature Communications, v. 8, 15887, https://doi.org/10.1038/ncomms15887.

Wang, X., Wang, B., Qiu, Z., Xie, G., Xie, J., Downs, W., Qiu, Z., and Deng, T., 2003, Danghe area (western Gansu, China) biostratigraphy and implications for depositional history and tectonics of northern Tibetan Plateau: Earth and Planetary Science Letters, v. 208, p. 253–269, https://doi.org/10.1016/S0012-821X(03)00047-5.

Wang, Y., Zheng, D., Pang, J., Zhang, H., Wang, W., Yu, J., Zhang, Z., Zheng, W., Zhang, P., and Li, Y., 2018, Using slope-area and apatite fission track analysis to decipher the rock uplift pattern of the Yumu Shan: New insights into the growth of the NE Tibetan Plateau: Geomorphology, v. 308, p. 118-128, https://doi.org/10.1016/j.geomorph.2018.02.006.

Yan, M., Van der Voo, R., Fang, X., Parés, J.M., and Rea, D.K., 2006, Paleomagnetic evidence for a mid-Miocene clockwise rotation of about 25° of the Guide Basin area in NE Tibet: Earth and Planetary Science Letters, v. 241, p. 234–247, https://doi.org/10.1016/j.epsl.2005.10.013.

Yin, A., Rumelhart, P.E., Butler, R., Cowgill, E., Harrison, T.M., Foster, D.A., Ingersoll, R.V., Zhang, Q., Zhou, X., Wang, X., Hanson, A., and Raza, A., 2002, Tectonic history of the Altyn Tagh fault system in northern Tibet inferred from Cenozoic sedimentation: Geological Society of America Bulletin, v. 114, p. 1257–1295, https://doi.org/10.1130/0016-7606(2002)114<1257:THOTAT>2.0.CO;2.

Yin, A., Dang, Y., Zhang, M., Chen, X., and McRivette, M.W., 2008, Cenozoic tectonic evolution of the Qaidam basin and its surrounding regions (Part 3): Structural geology, sedimentation, and regional tectonic reconstruction: Geological Society of America Bulletin, v. 120, p. 847–876, https://doi.org/10.1130/B26232.1.

Yu, J.X., Zheng, W.J., Kirby, E., Zhang, P.Z., Lei, Q.Y., Ge, W.P., Wang, W.T., Li, X.N., and Zhang, N., 2016, Kinematics of late Quaternary slip along the Yabrai fault: Implications for Cenozoic tectonics across the Gobi Alashan block, China: Lithosphere, v. 8, p. 199–218, https://doi.org/10.1130/L509.1.

Yuan, D., Ge, W., Chen, Z., Li, C., Wang, Z., Zhang, H., Zhang, P., Zheng, D., Zheng, W., and Craddock, W.H., 2013, The growth of northeastern Tibet and its relevance to large-scale continental geodynamics: A review of recent studies: Tectonics, v. 32, p. 1358–1370, https://doi.org/10.1002/tect.20081.

Yue, Y., and Liou, J.G., 1999, Two-stage evolution model for the Altyn Tagh fault, China: Geology, v. 27, p. 227–230, https://doi.org/10.1130/0091-7613(1999)027<0227:TSEMFT>2.3.CO;2.

Zhang, P., Burchfiel, B.C., Molnar, P., Zhang, W., Jiao, D., Deng, Q., Wang, Y., Royden, L., and Song, F., 1991, Amount and style of late Cenozoic deformation in the Liupan Shan area, Ningxia Autonomous Region, China: Tectonics, v. 10, p. 1111–1129, https://doi.org/10.1029/90TC02686.

Zhao, Z., Fang, X., and Li, J., 2001, Late Cenozoic magnetic polarity stratigraphy in the Jiudong Basin, northern Qilian Mountain: Science in China, Series D: Earth Sciences, v. 44, p. 243–250, https://doi.org/10.1007/BF02911993.

Zheng, D., Zhang, P., Wan, J., Yuan, D., Li, C., Yin, G., Zhang, G., Wang, Z., Min, W., and Chen, J., 2006, Rapid exhumation at ~8 Ma on the Liupan Shan thrust fault from apatite fission-track thermochronology: Implications for growth of the northeastern Tibetan Plateau margin: Earth and Planetary Science Letters, v. 248, p. 198–208, https://doi.org/10.1016/j.epsl.2006.05.023.

Zheng, D., Clark, M.K., Zhang, P., Zheng, W., and Farley, K.A., 2010, Fault initiation, topographic growth and erosion rates of the northern Tibetan Plateau (Qilian Shan): Geosphere, v. 6, p. 937–941, https://doi.org/10.1130/GES00523.1.

Zheng, D., Wang, W., Wan, J., Yuan, D., Liu, C., Zheng, W., Zhang, H., Pang, J., and Zhang, P., 2017, Progressive northward growth of the northern Qilian Shan–Hexi Corridor (northeastern Tibet) during the Cenozoic: Lithosphere, v. 9, p. 408–416, https://doi.org/10.1130/L587.1.

Zheng, W., Zhang, P., Ge, W., Molnar, P., Zhang, H., Yuan, D., and Liu, J., 2013, Late Quaternary slip rate of the South Heli Shan Fault (northern Hexi Corridor, NW China) and its implications for northeastward growth of the Tibetan Plateau: Tectonics, v. 32, p. 271–293, https://doi.org/10.1002/tect.20022.

Zhuang, G., Johnstone, S.A., Hourigan, J., Ritts, B., Robinson, A., and Sobel, E.R., 2018, Understanding the geologic evolution of Northern Tibetan Plateau with multiple thermochronometers: Gondwana Research, v. 58, p. 195–210, https://doi.org/10.1016/j.gr.2018.02.014.



Downloaded from http://pubs.geoscienceworld.org/gsa/geosphere/article-pdf/15/2/423/4663892/423.pdf
by guest